Progress In Electromagnetics Research M, Vol. 56, 197–205, 2017

Design of Ultrathin Absorptive/Transmissive Radome with Dual Passbands

Bo Yi*, Peiguo Liu, and Gaosheng Li

Abstract—An ultrathin absorptive/transmissive radome with dual passbands is presented in this paper. The total thickness of radome is only 5 mm. The dual passbands are located at around 1.05 GHz and 2.2 GHz, respectively. The absorbing band ranges from 6.28 GHz to 15.04 GHz for TE wave incidence and from 6.3 GHz to 15.16 GHz for TM wave incidence. Due to the miniaturized elements, the grating lobes are shifted out of absorbing band to higher frequency. Both numerical and experimental results are also given out.

1. INTRODUCTION

A radome can protect the antenna against malfunctions or serious damages caused by debris or ice. Other than protecting radiating elements from their physical environment, another crucial important function is to reduce the Radar Cross Section (RCS) [1]. Frequency selective surface (FSS) could transmit the in-band wave and reflect the out-of-band power to other unimportant direction. The reflecting signal may also be detected by multistatic radar system, hence this approach can be classified as a fictitious RCS reduction technique [2].

Different from traditional FSS, an absorptive/transmissive FSS was proposed firstly in a patent [3]. According to the patent, the absorptive/transmissive structure could reduce the electromagnetic signature of the radome and antenna without disrupting the electromagnetic waves generated by the antenna, while absorbing the energy of electromagnetic wave at a particular frequency or range of frequencies. However, this patent only stated the working principle of the radome, and no any quantitative results were presented.

Costa and Monorchio synthesized an absorptive/transmissive radome using designed resistive surface and metallic periodic surface [1]. Zhou et al. designed and fabricated another absorptive/transmissive radome using magnetic material. Its transmitting and absorbing properties were verified by simulation and experiments [4]. Liu et al. proposed and manufactured an absorptive/transmissive radome using resistors loaded double square loop (DSL) and convoluted slot [2]. Chen and Fu verified its performance and influence on antenna using a planar antenna [5]. They improved the radome by replacing the resistors loaded DSL metal layers and convoluted slots with resistors loaded incurved square loop (ISL) and miniaturized FSS, respectively [6]. They also designed an absorptive frequency selective surface with good transmission at high frequency [7, 8]. All the above structures had only one passband. But in modern society, many equipments, such as mobile phone, have two or more working frequencies. In other words, two or more passbands are needed in order to guarantee their normal operation.

In this contribution, a dual-passband absorptive/transmissive radome was proposed. Compared to the previous works in [9], one more passband is proposed. The resistors loaded DSL metal layer, instead

Received 11 February 2017, Accepted 27 April 2017, Scheduled 16 May 2017

* Corresponding author: Bo Yi (yibo_nudt@nudt.edt.cn).

The authors are with the College of Electronic Science and Engineering, National University of Defense Technology, Changsha 410073, China.

of resistive surface, is used as resistive FSS, which is insensitive to polarization of incident wave [10]. Capacitors are loaded on the bandpass FSS to reduce the unit size, hence the grating lobes are shifted out of absorbing band to higher frequency. The periods of resistive and bandpass FSS are 10 mm and 15 mm, respectively. The dual passbands are located at 1.05 GHz and 2.2 GHz, Which can be used for communication. The passband frequencies can be shifted by adjusting the structural parameters and loaded capacitance. The radome, whose thickness is only 5 mm, has low profile, and the absorptive band ranges from 6.28 GHz to 15.04 GHz for TE wave incidence and from 6.3 GHz to 15.16 GHz for TM wave incidence.

The paper is organized as follows. In Section 2, after brief description of the fundamental circuit of microwave filter with dual passbands, the capacitors loaded dual-passband FSS is used to design ultrathin absorptive/transmissive radome. Related simulated results for radome are also given. A prototype of the designed radome is fabricated, and the measurement is carried out to verify the performance of the designed radome in Section 3. Conclusions are drawn in Section 4.

2. RADOME DESIGN AND SIMULATION

An absorptive/transmissive radome often consists of resistive FSS, substrate and bandpass FSS. In order to maximize the transmission coefficients around transmitting frequency, the resonant frequency of bandpass FSS and resistive FSS should keep a distance with each other. The substrate will impact the starting frequency of absorbing band. The thicker the substrate is, the lower the starting frequency is [11]. The permittivity of substrate also has influence on the width of absorbing band. Lower permittivity corresponds to wider absorbing band.

For the structure whose the starting frequency of absorbing band is higher than the transmitting frequency, the bandpass FSS should adopt miniaturized unit cells to avoid grating lobes appearing in the absorbing band. Loading lumped capacitors is one of the methods to reduce the period of the unit cell and improve the stability as the incident angle increases [12–15]. On the other hand, the location of passband might be easily adjusted by changing the loaded capacitance.

There are three important steps to synthesize an absorptive/transmissive radome with dual passbands. The first and second steps are to design resistive FSS and select proper material as substrate. The third step is to design the bandpass FSS with dual passbands and wide reflecting property. The designed resistive and bandpass FSS should better be rotationally symmetric to guarantee the polarization independent property. The permittivity of substrate should better be low to enlarge the absorbing band.

The resistors loaded DSLs are used as resistive FSS owning to its rotational symmetry. Fig. 1 shows the fundamental circuit of microwave filter with dual passbands, which form the foundation of synthesizing bandpass FSS. The first passband is decided by capacitance C_1 and inductance L_1. The second passband is decided by the capacitance C_2, inductance L_2 and inductance L_1.

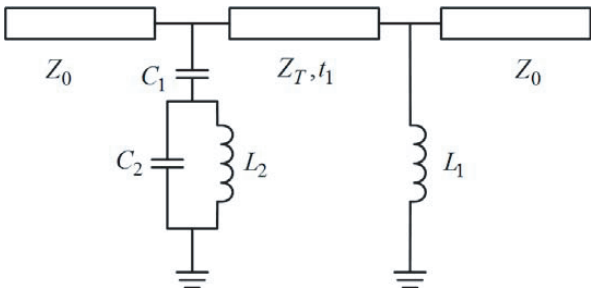

Figure 1. The basic equivalent circuit of microwave filter with dual passband.

The 3D view of designed radome is shown in Fig. 2(a). The radome consists of two layers of FSS separated by a substrate with thickness t_1. Fig. 2(b) shows the compositions of resistive FSS. The two layers of bandpass FSS are presented in Fig. 2(c) and Fig. 2(d). The metal grid in Fig. 2(c) shows an

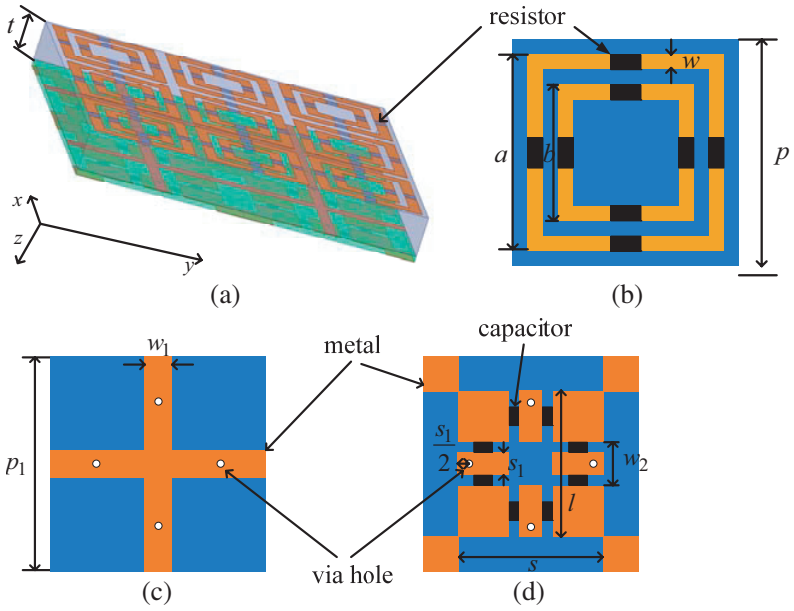

Figure 2. Geometries for unit cell of radome. (a) 3D view, (b) structure of resistive FSS, (c) (d) structure of bandpass FSS.

inductive behavior and acts as inductor L_1 in equivalent circuit when interacting with normal incident electromagnetic wave. The inductance might be adjusted by changing the width w_1 of metal grid. The inductor L_2, capacitor C_1 and capacitor C_2 of equivalent circuit in Fig. 1 are presented in the bandpass FSS in Fig. 2(d). In order to reduce the unit size and maintain the angle stability, capacitors are loaded on it.

The parameters of radome are listed in Table 1, and all of them are optimized by the CST. The resistances of inner and outer loops, which have influence on the absorbing property, are 1000 Ω and 300 Ω, respectively. The radius of via holes penetrating the bandpass FSS is 0.4 mm. The loaded capacitance on the bandpass FSS is 1.8 pf, and the thickness t of the substrate is equal to 4.5 mm. The thickness of passband FSS is 0.5 mm. The parameters keep unchangeable in simulation unless specially declaring.

Table 1. Structural parameters list of designed radome.

parameters	p	p_1	a	b	w	w_1	l	s	s_1	w_2
Value(mm)	10	15	8.5	5.5	1	1.5	12	10	1.5	3.5

The resistors have two main functions [16]. Firstly, they act as impedance transformer in absorbing band. When the impedance of radome equals that of free space, the reflecting energy reaches minimum value. Secondly, the resistors will absorb the incident electromagnetic wave. The loaded capacitors are to increase the capacitance of bandpass FSS and shrink the period of bandpass FSS. They have little influence on the absorbing band.

Figure 3 shows the influence of loaded capacitance, width of metal grid and slot to the frequencies of two passband. The results in Fig. 3 are obtained by simulation only for the passband FSS. From Fig. 3, we can know that as loaded capacitance increases and width of metal grid becomes narrower, both of the passbands shift to lower frequency. As the width of slot increases, only the second passband shifts to lower frequency. From the above analysis, we can conclude that in order to get desired passband frequencies, the first step is to adjust the width of metal grid and loaded capacitance to get designed frequency of the first passband. The second step is to adjust the width of slot to get the desired frequency of the second passband.

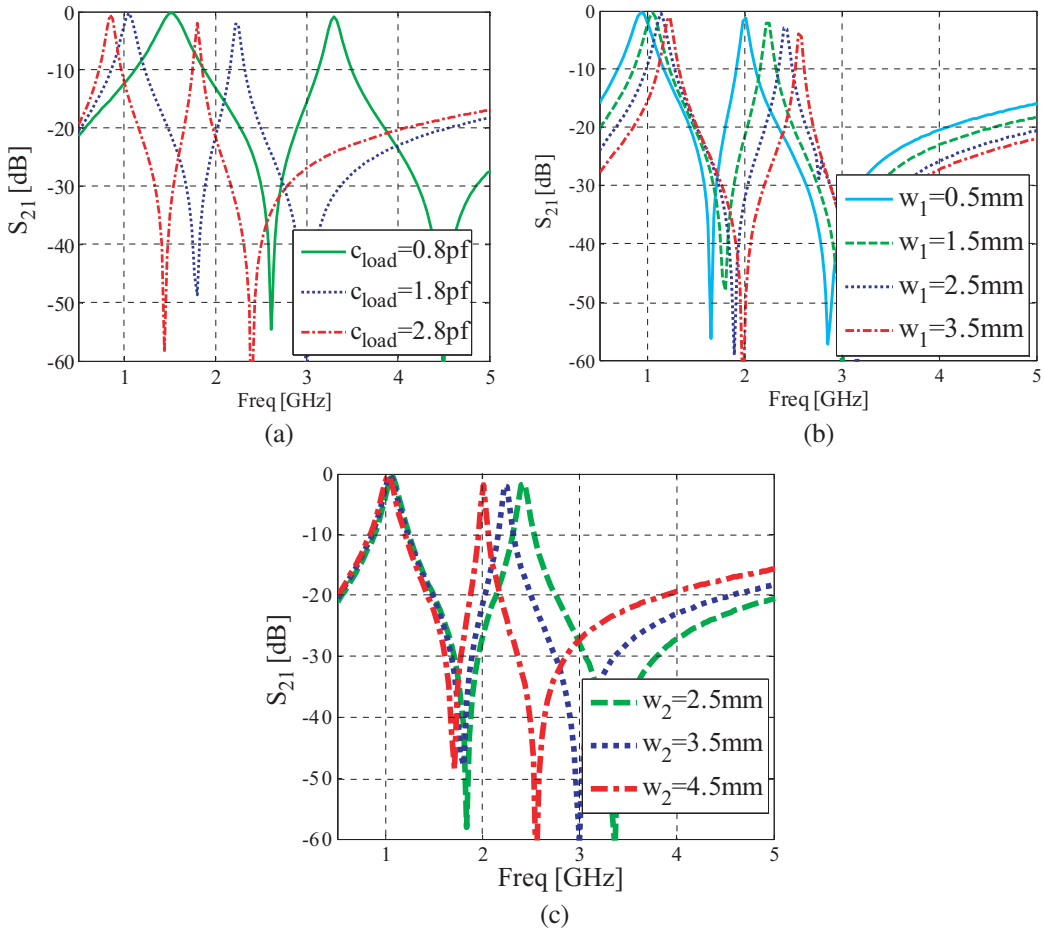

Figure 3. The influence of structural parameters and loaded capacitance to the two passband. (a) Loaded capacitance, (b) width w_1 of metal grid, (c) width w_2 of slot.

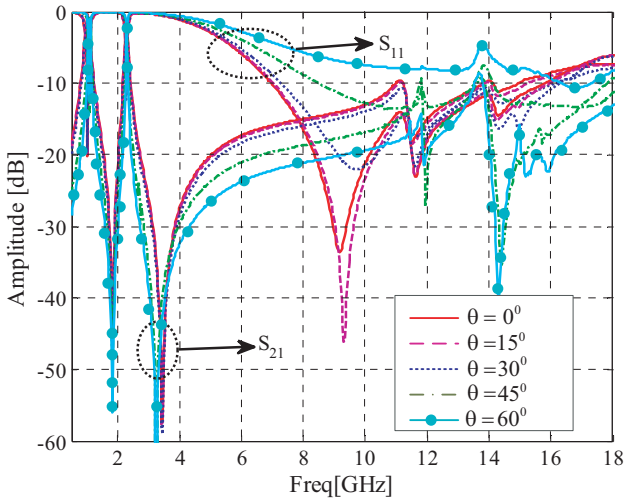

Figure 4. Simulated transmission and reflection coefficients.

Figure 4 shows simulated transmission and reflection coefficients of the radome with different angles incidences. In simulation, the boundaries of X and Y directions are set as unit cell and that of Z direction set as open (add space). The dual passbands are located at around 1.05 GHz and 2.28 GHz.

Their insertion losses are −0.4 dB at 1.05 GHz and −1.3 dB at 2.28 GHz. The absorbing band ranges from 6.9 GHz to 15 GHz. From Fig. 4, it can also be found that both passbands and absorbing band almost keep stability as the incident angle increases to 45. But as the incident angle goes on increasing up to 60, the bandwidth of absorbing band decreases.

The comparisons of simulated bistatic reflections between a metal sheet and finite radome at different frequencies, performed on personal computer, are presented in Fig. 5. The oblique incident angle is 45°. The size of both simulated radome and metal sheet are 180 mm × 180 mm. In Fig. 5, the dash and solid lines denote the reflection coefficients of metal sheet and radome, respectively. As shown in Fig. 5, compared to the metal sheet, the bistatic reflection of radome is reduced obviously, especially in the specular directions. Further, no grating lobes appear in the absorbing band.

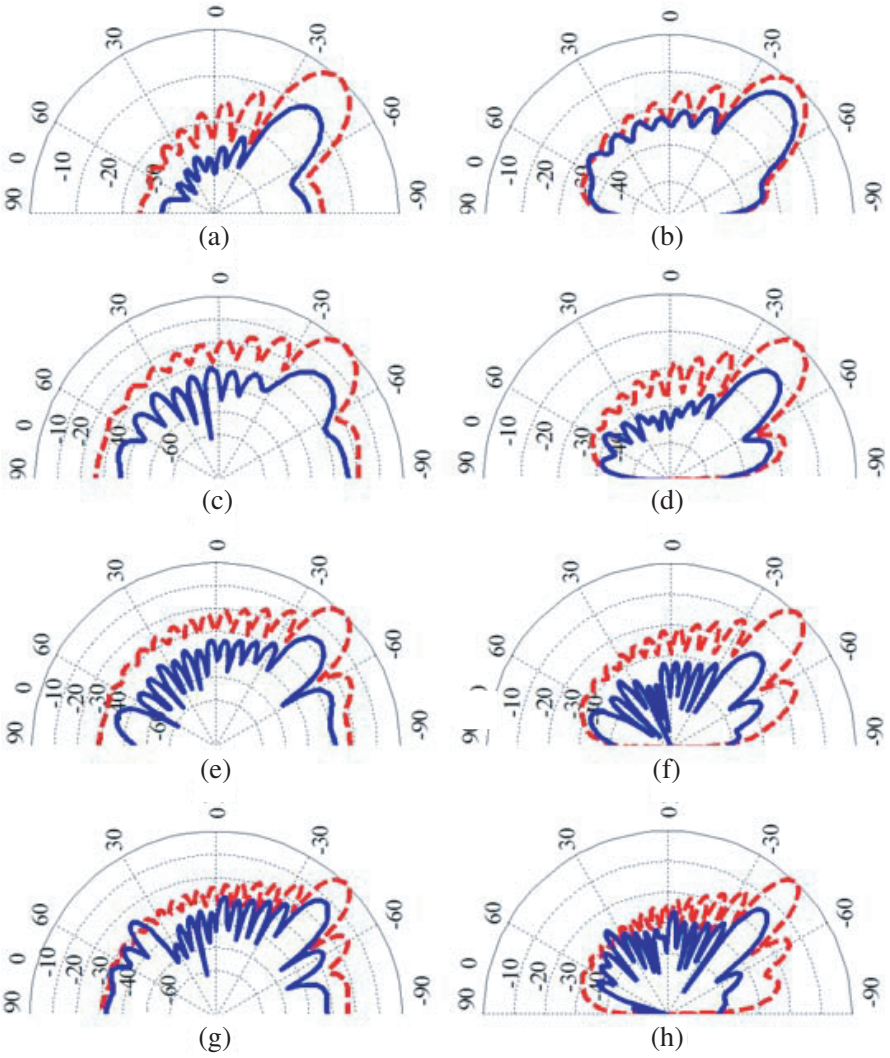

Figure 5. Comparison of simulated bistatic reflection between a metal sheet and a finite radome. (a) TE 7 GHz, (b) TM 7 GHz, (c) TE 9 GHz, (d) TM 9 GHz, (e) TE 12 GHz, (f) TM 12 GHz, (g) TE 15 GHz, (h) TM 15 GHz.

From the above simulated results, the design procedures of radome can be summarized as follows.

Firstly, select filtering circuit with two passbands and construct the corresponding structure.

Secondly, adjust the parameters of structure and loaded capacitance based on the above results to meet the design requirement.

3. EXPERIMENTAL RESULTS

A prototype, as shown in Fig. 6, is fabricated using printed circuit technology to verify the performance of designed radome. The dimension of manufactural radome is 300 mm × 300 mm, which contains 20 × 20 unit cells for bandpass FSS and 30 × 30 unit cells for resistive FSS. Both the resistive and bandpass FSSs are printed on the Rogers Ro4350 with $\xi_r = 3.48$ and thickness 0.5 mm. PMI foam ($\xi_{r1} = 1.12$ and thickness 4.5 mm) is used as substrate.

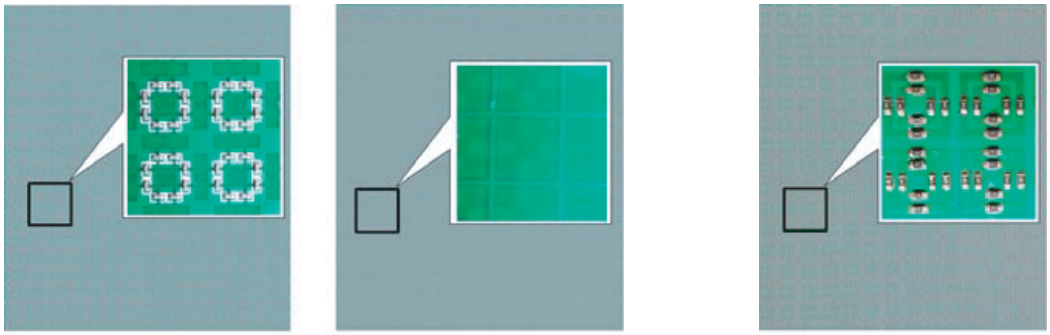

(a) (b)

Figure 6. Photograph of radome. (a) Bandpass FSS, (b) resistive FSS.

A photograph of experimental setup is shown in Fig. 7. A wooden fixture, which is put in the middle of two ridged horn antennas, is built. It is windowed at its center and covered with absorbing material. The side length is 1.5 m. The operation band of the two horn antennas is from 1 GHz to 18 GHz. The left antenna is used as transmitting antenna, and the right one is used as receiving antenna. To guarantee that the radome is excited by plane wave, the distance between horn antenna and fixture is set to 0.6 m. The vector network analyzer Anritsu (VNA) Ms4642A is employed to measure the reflection and transmission coefficients of the designed radome.

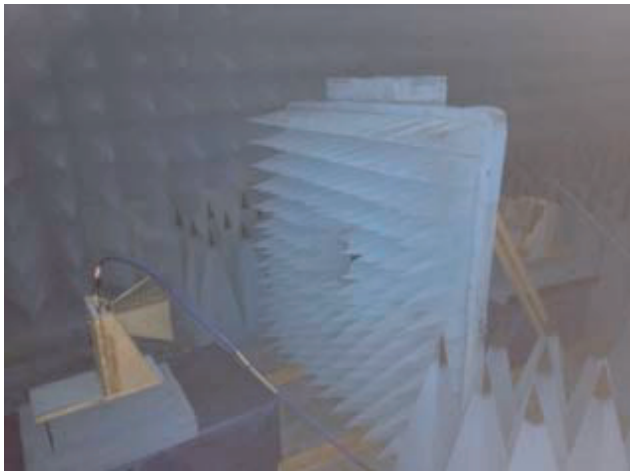

Figure 7. Photograph of experimental setup.

Figure 8 shows the simulated and measured transmission coefficients of the radome with different incident angles. The simulated results agree well with the measured ones. The measured transmission frequencies are located at 1.05 GHz with insertion loss −1.04 dB and 2.2 GHz with insertion loss −2.3 dB. The small deviations between simulated and measured results may be ascribe to the substrate of PMI foam, which is regarded as free space in simulation.

The simulated and measured absorbing properties of the radome are shown in Fig. 9. As shown in Fig. 9, the measured absorbing band ranges from 6.28 GHz to 15.04 GHz for TE wave incidence and from 6.3 GHz to 15.16 GHz for TM wave incidence. The measured bandwidth almost agrees with simulated ones. The absorbing properties keep stability as the incident angle increases. Compared to the simulated absorbing band, the starting frequency of measured ones moves to lower frequency. As the frequency increases, the deviation between simulated and measured results becomes more obvious.

The discrepancies between simulated and measured results in Fig. 8 and Fig. 9 may owe to fabrication error and measurement situation. The soldering of diodes and resistors will have disparity from each other, and the size of the fabricated radome is also finite. The measurement errors also have influence on the discrepancies. The electromagnetic wave, which reaches the receiving antenna by detouring around the edge of absorbing wall, will impact the accuracy of transmission coefficients. Compared to measurement for the transmission coefficients, the test for reflection coefficient is more sensitive to the experimental arrangement. The reason is that the reflecting power is much lower than transmission ones. Furthermore, the parasitic effects of packaging may also lead to the deviation between simulated and measured results. In low frequency, parasitic effects of resistor and capacitor are

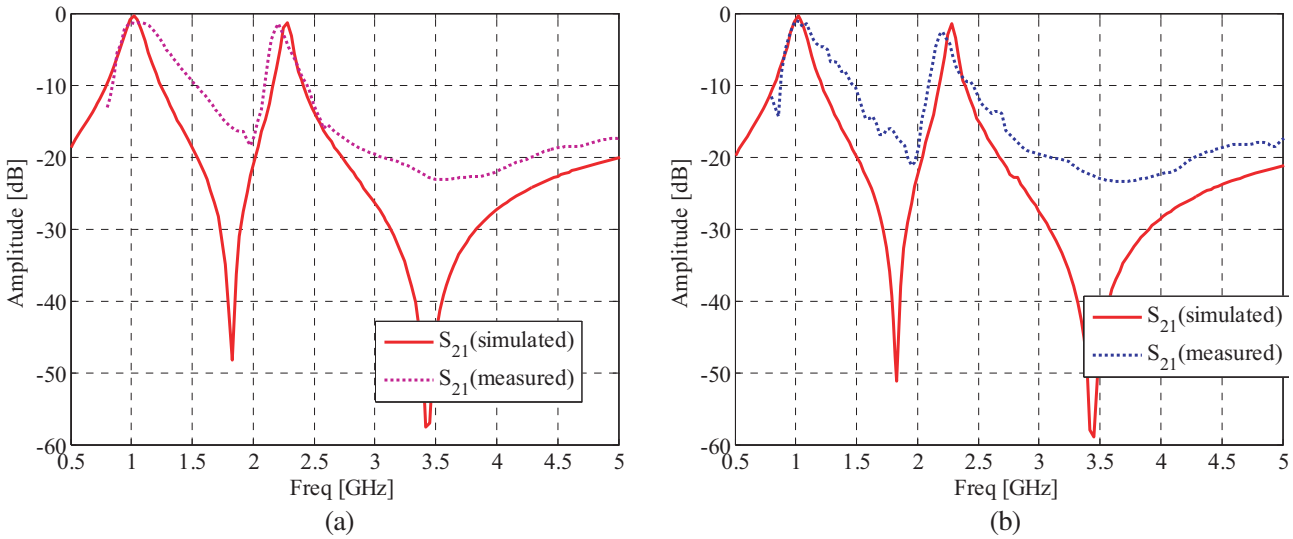

Figure 8. The simulated and measured passband of the designed radome with different incident angle. (a) 15°, (b) 30°.

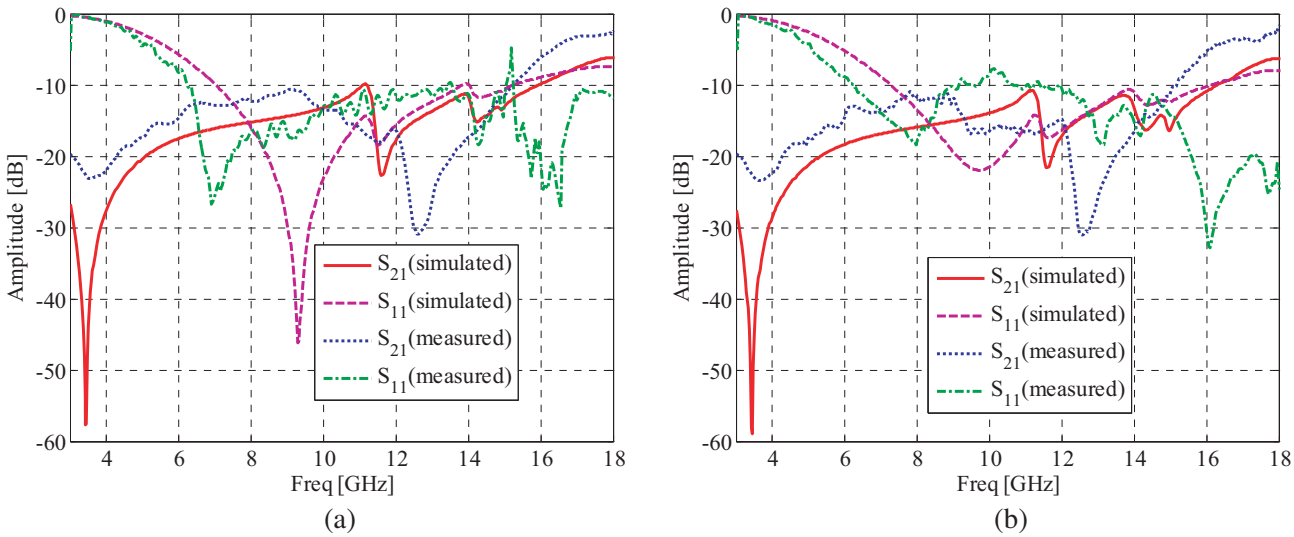

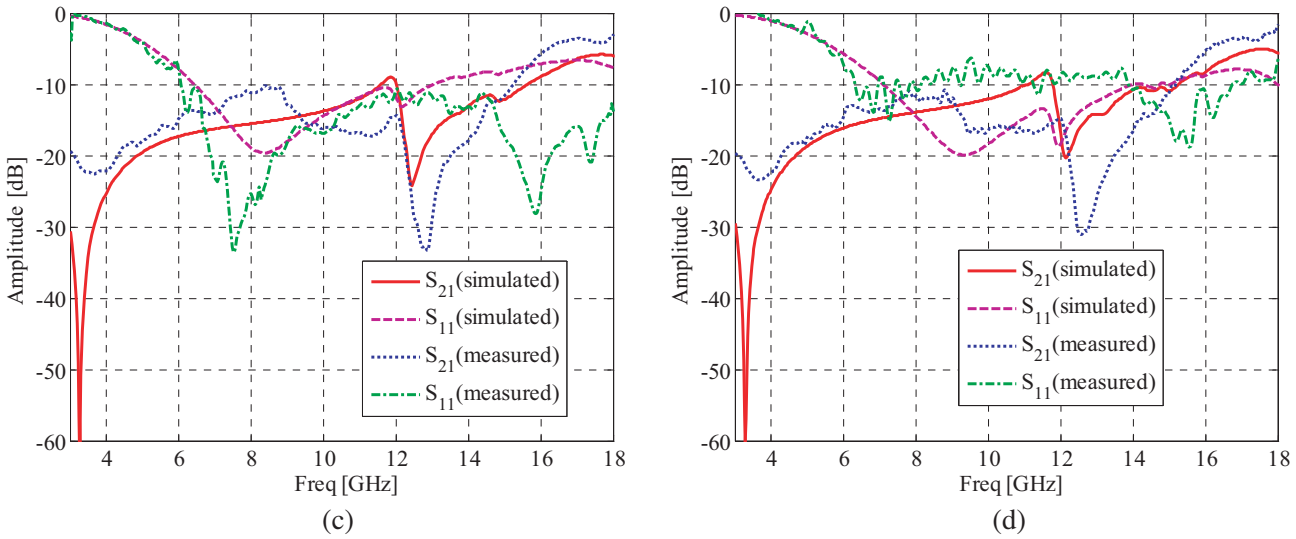

Figure 9. The simulated and measured absorbing properties of designed radome. (a) TE 15°, (b) TE 30°, (c) TM 15°, (d) TM 30°.

not considered. But as frequency increases, the parasitic capacitance and inductance should be taken into account.

4. CONCLUSION

In this paper, a miniaturized absorbing/transmissive radome with dual passbands is proposed and fabricated. The experiments show that the dual passbands are located around 1.05 GHz and 2.2 GHz, which agree well with the simulated ones. The absorbing band of the radome ranges from 6.28 GHz to 15.04 GHz for TE wave incidence and from 6.3 GHz to 15.16 GHz for TM wave incidence. The absorbing properties keep stability as the incident angle increases. Due to the miniaturized element, the grating lobes are shifted out of absorbing band to higher frequency. Because of parasitic effects of packaging and measurement errors, the simulated results deviate from the measured ones at high frequency.

REFERENCES

1. Costa, F. and A. Monorchio, "A frequency selective raome with wideband absorbing properties," *IEEE Transactions on Antennas and Propagation*, Vol. 60, No. 6, 2740–2747, 2012.
2. Liu, L., Y. Li, Q. Meng, et al., "Design of an invisible radome by frequency selective surface loaded with lumped resistors," *Chin. Phys. Lett.*, Vol. 30, No. 6, 064101, 2013.
3. Arceneaux, W. S., R. D. Akins, and W. B. May, "Absorptive/transmissive radome," US Patent 5,400,043,1995.
4. Zhou, H., L. Yang, S. Qu, et al., "Experimental demonstration of an absorptive/transmissive FSS with magnetic material," *IEEE Antennas and Wireless Propagation Letters*, Vol. 13, 114–117, 2014.
5. Chen, Q. and Y. Fu, "A planar stealthy antenna radome using absorptive frequency selective surface," *Microwave and Optical Technology Letters*, Vol. 56, No. 8, 1788–1792, 2014.
6. Chen, Q., J. Bai, L. Chen, and Y. Fu, "A miniaturized absorptive frequency selective surface," *IEEE Antennas and Wireless Propagation Letters*, Vol. 14, 80–83, 2015.
7. Chen, Q., L. Chen, J. Bai, and Y. Fui, "Design of absorptive frequency selective surface with good transmission at high frequency," *Electronics Letters*, Vol. 51, 885–886, 2015.
8. Chen, Q., L. Liu, L. Chen, J. Bai, and Y. Fu, "Absorptive frequency selective surface using parallel LC resonance," *Electronics Letters*, Vol. 52, 418–419, 2016.

9. Yi, B., L. Yang, and P. Liu, "Design of miniaturized and ultrathin absorptive/transmissive radome based on interdigital square loops," *Progress In Electromagnetic Research Letters*, Vol. 62, 2016, 117–123.
10. Kartal, M. and B. Doken, "A new frequency selective absorber surface at the unlicensed 2.4-GHz ISM band," *Microwave and Optical Technology Letters*, Vol. 58, No. 10, 2351–2358, 2016.
11. Munk, *Frequency Selective Surface: Theory and Design*, Wiley, New York, 2000.
12. Liu, H. L., K. L. Ford, and R. J. Langley, "Design methodology for a miniaturized frequency selective surface using lumped reactive components," *IEEE Transactions on Antennas and Propagation*, Vol. 57, 2732–2738, 2009.
13. Liu, H. L., K. L. Ford, and R. J. Langley, "Miniaturized bandpass frequency selective surface with lumped components," *Electronics Letters*, Vol. 44, 1–2, 2008.
14. Xu, R. R., H. C. Zhao, Z. Y. Zong, and W. Wu, "Dual-band capacitive loaded frequency selective surfaces with close band spacing," *IEEE Microwave and Wireless Components Letters*, Vol. 18, 782–784, 2008.
15. Ebrahimi, A., W. Withayachumnankul, S. Al-Sarawi, and D. Abbott, "Design of dual band frequency selective surface with miniaturized elements," *The 2014 International Workshop on Antenna Technology*, 201–204, 2014.
16. Han, Y., W. Che, and Y. Chang, "Investigation of thin and broadband capacitive surface based absorbers by the impedance analysis method," *IEEE Transactions on Electromagnetic Compatibility*, Vol. 57, No. 1, 22–26, 2015.